Journal of Applied Physics ARTICLE pubs.aip.org/aip/jap

Universal strain engineering for enhancing the hole mobility and dopability in *p*-type semiconductors

Cite as: J. Appl. Phys. **136**, 015701 (2024); doi: 10.1063/5.0210247
Submitted: 25 March 2024 · Accepted: 9 June 2024 ·
Published Online: 2 July 2024

Yaoqiao Hu and Kyeongjae Cho[a)]

AFFILIATIONS

Department of Materials Science and Engineering, The University of Texas at Dallas, Richardson, Texas 75080, USA

[a)]**Author to whom correspondence should be addressed:** kjcho@utdallas.edu

ABSTRACT

Modern electronic and optoelectronic devices rely on the development of the complementary pair of *n*-type and *p*-type semiconductors. However, it is often seen that *n*-type semiconductors are easier to realize and offer superior performances than their *p*-type counterparts, with *p*-type semiconductors showing much lower hole mobility and inefficient carrier doping. Here, by using first-principles studies, we demonstrate that lattice strain engineering can be a universal approach to enhance the hole mobility and dopability in *p*-type semiconductors. A broad class of *p*-type semiconductors, including anion *p* orbital derived valence band compounds (nitrides, oxides, halides, and chalcogenides), *s* orbital based post-transition metal oxides (e.g., SnO), and *d*-orbital based transition metal oxides (e.g., NiO), have been applied on strain to demonstrate their valence band modulation ability for the purpose of increasing the hole mobility and *p*-type dopability. We show that compressive lattice strain generally results in an upshifted valence band edge and reduced effective hole mass, leading to enhanced *p*-type dopability and increased hole mobility. Our work highlights strain engineering as a universal and effective approach for achieving better performed *p*-type compound semiconductors.

I. INTRODUCTION

Complementary pairs of *n*-type and *p*-type semiconductors are the materials basics of electronic devices such as MOSFETs and optoelectronic devices like LEDs. Our nature has its propensity that *n*-type semiconductors seem easier to realize and offer superior performances than their *p*-type counterparts: Si has larger electron mobility than hole mobility, and an *n*-channel Si MOSFET generally has a higher drive current than a *p*-channel Si MOSFET. This is even more true when it comes to compound semiconductors.[1,2] GaN has been commercially used for blue LEDs and high-power devices due to its high breakdown field, high electron mobility, and high thermal stability;[1] nevertheless, most GaN based devices are limited to *n*-type conduction with the *p*-type device performances lagging far behind due to its low hole mobility and inefficient *p*-type doping. Until now, there does not exist efficient *p*-type dopants for GaN, which can induce high *p*-type conductivity.[3] Even the most widely investigated acceptor Mg possesses much higher substitution formation energy and deeper activation energy level [~200 meV above the valence band edge (VBE)] than typical shallow acceptors in conventional semiconductors.[3,4] Developing high-mobility and high dopability *p*-type semiconductors would enable a complementary solution that provides more flexibility for the design and implementation of more efficient electronics and optoelectronics.

There are fundamental issues with compound semiconductors that prevent them from being implemented as *p*-type semiconductors. Taking GaN as an example, its bottom conduction band derives mainly from metal's *s* orbital (Ga-4*s*) and top valence band is contributed mostly from anion's *p* orbital (N-2*p*). Such orbital characteristics at the band edges result in several critical issues in terms of *p*-type conduction performance. First, the anion's *p* orbitals tend to be localized and result in heavy hole (HH) effective mass; as a result, the hole carriers exhibit low mobilities. In contrast, metal cation's *s* orbitals are typically more delocalized, which generally leads to stronger conduction band dispersion and smaller effective mass of electrons. Second, anion's *p* orbitals, due to their

large electronegativity, typically lead to deep-lying valence band edges. This leads to the hole-compensating intrinsic defects to form spontaneous under high p-doping conditions.[5–7] In addition, they are difficult to be doped with shallow dopants that possess an ionization energy level right above the valence band edge (VBE). Third, due to the deep valence band edge, a high Schottky barrier to contact metal with high contact resistance is expected. This scenario is generally applicable to other wide bandgap compound semiconductors including nitrides, oxides, halides, and chalcogenides.

One possible way to overcome these issues is to engineer raising up the VBE energy level and reduce the hole effective mass through modifying the electronic band structure. Strain has been widely adopted in engineering the band structure for better performed materials,[8–10] as seen in strained Si technology for higher hole mobility in the p-channel MOSFET[8] and in graphene for opening bandgap for logic transistor application.[11] More recently, strain engineering has been intensively investigated to enhance the thermoelectric performance of thermoelectric materials,[12–16] to induce the metal–insulator transition,[17] to modulate the ferromagnetism,[18] and to modulate the metal contact Schottky barrier.[19] Sporadically, strain engineering has also been applied to enhance the p-type semiconductor performance, which includes enhancing the hole mobility[20] and decreasing the acceptor ionization energy.[21,22] In particular, strain engineering has been applied on GaN for HEMT devices[23] as well as for hole carriers.[24] It is worthwhile to investigate the strain effect on the band structures of compound semiconductors, specifically on whether the strain engineering could result in a more dispersive and shallower top valence band for high hole mobility and p-type dopability. From a tight binding point of view, the band dispersion is due to the interatomic orbital overlap interaction. Therefore, engineering the atomic distance by strain will alter the atomic orbital overlap interaction strength and, thus, the band dispersion structure. Strain engineering to tailor the valence band edge for better p-doping capability and high hole mobility would be highly potential for p-type semiconductors technology development.

In this work, by using density functional theory (DFT) based first-principles calculations, we investigate the band structure engineering via strain for high hole mobility and p-type dopability in compound semiconductors. We will show that under compressive strain, a wide range of compound semiconductors, including nitrides, chalcogenides, halides, post-transition metal oxides, transition metal oxides, and mixed-anions oxides, all exhibit VBE upshifting and hole effective mass decreasing. This leads to better p-type conduction performance with high hole mobility and good p-type dopability. We will demonstrate that strain engineering could be a universal way to engineer the band structures in compound semiconductors for better performed p-type semiconductors.

II. COMPUTATIONAL METHOD

DFT-based first-principles calculations were performed by using Vienna *Ab initio* Simulation Package (VASP),[25,26] which uses projector augmented wave and pseudopotentials.[27,28] Generalized gradient approximation with Perdew–Burke–Ernzerhof (GGA-PBE) type functional[29] was employed to calculate the electronic exchange-correlation potential energy. For all calculations, a cutoff energy of 520 eV was used for plane-wave basis expansion. Brillouin zone k-point sampling was based on the Monkhorst–Pack scheme,[30] with the k-mesh grid density varying according to the supercell size to ensure the desired accuracy of greater than 0.03/Å. For structure relaxation, a conjugate gradient method was employed,[31] with the stopping criterion being the force on each atom being less than 0.01 eV/Å. Electronic minimizations were achieved by blocked-Davidson iteration algorithm,[32] with the convergence criteria being the energy difference between two consecutive iterations less than 10^{-5} eV. For projected density of states (DOS) calculation, the wave function was projected onto each atom by calculating the inner product of the wave function and spherical function.

Effective masses are calculated using the parabolic approximation of the valence band maxima, where the effective mass is related to the second derivative in the E–k curve: $m^* = \hbar^2/\left(\frac{d^2E}{dk^2}\right)$. Hole mobility, on the other hand, is a quantity whose calculation requires complex electron–phonon coupling evaluation and demands significant computational resources. Given that the carrier mobility is strongly related to its effective mass, in this work the effective masses are used to estimate the hole mobilities of p-type semiconductors. Such practice has been seen in previous works where small effective mass is the key factor for a high motility.[2,6,33] Throughout the work, we will focus on the effect of lattice strain on the effective mass to reveal the hole mobility mouldability under strain engineering.

Lattice strains were applied by changing the lattice constants of unit cells. Atomic positions were then allowed to relax with the cell size fixed. The acceptor activation energy was calculated based on the defect formation energy computation. For defect calculations, supercell technique was adopted. The formation energy of defect D in charged state q, $E^f[D^q]$, can be written as[34]

$$E^f[D^q] = E_{\text{def}}[D^q] - E_{\text{bulk}} - \sum n_i\mu_i + q(E_F + E_{\text{VBM}}) + E_{\text{corr}}[D^q],$$

where $E_{\text{def}}[D^q]$ is the energy of the supercell with defects, E_{bulk} is the energy of the perfect supercell without any defects, n_i indicates the number of the ith-atoms that have been added into ($n_i > 0$) or removed from ($n_i < 0$) the supercell, and μ_i is the chemical potential of defective atoms. E_{VBM} is the energy of the VBE, and E_F is the Fermi level referenced to E_{VBM}. The correction term $E_{\text{corr}}[D^q]$ is introduced to account for the spurious interactions between the charges and their images. In our work, the defect states with the charge q were corrected using the Freysoldt scheme,[35] as implemented in the PyCDT package.[36]

III. RESULTS AND DISCUSSION

A. Nitrides: GaN

We first investigate the strain effect on wurtzite GaN (wz-GaN) for p-type conduction. The wz-GaN structure consists of alternating hexagonal-closed-packed (0001) Ga and N layers[(Figs. 1(a) and 1(b)]. In terms of a local bonding environment, each Ga is tetrahedrally coordinated to four N atoms and vice versa. Figure 1(d) shows the calculated band structure at the DFT-PBE level with bandgap corrected by rigid band edge shifting. The conduction band edge is mainly contributed by the Ga-s orbital, and the valence band edge is

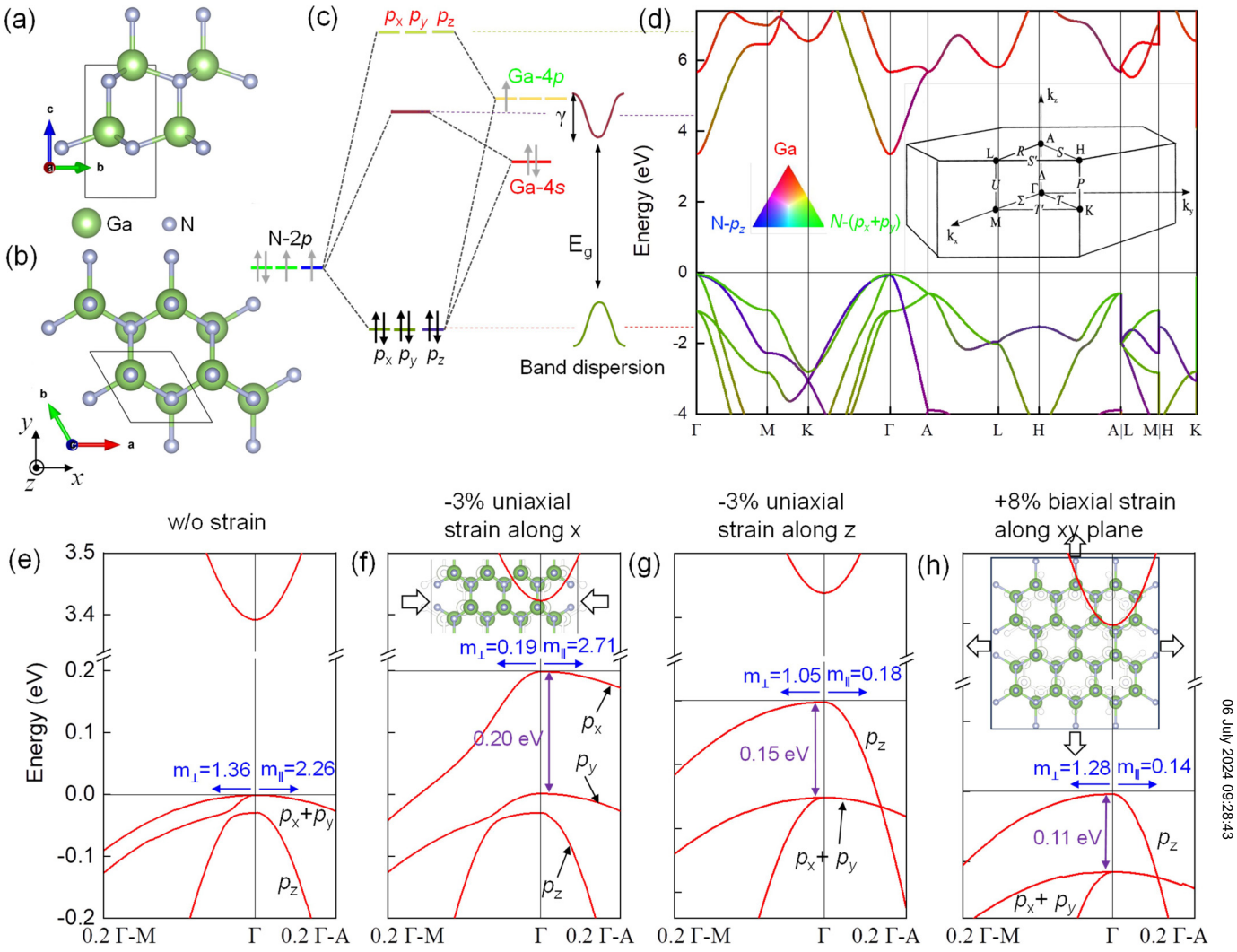

FIG. 1. Atomic structure of wz-GaN in (a) side view and (b) top view. (c) Molecular orbital diagrams and (d) band structure of wz-GaN. The dashed line is used to show the connection between the molecular orbitals and energy bands in the band structure. Due to the orbital overlap interaction, the molecular orbital energy disperses up and down forming the energy band, with the original molecular orbital energy level being the center position of the band. A schematic band dispersion of the bottom conduction band and top valence band is plotted. The band structure is computed under the DFT-GGA level. A rigid band edge shift was applied to reproduce the experimental bandgap. The Brillouin zone of wurtzite GaN is given as an inset. A color scheme is used to visualize the atomic orbital contribution to each band. (e)–(h) Valence band structure details along Γ-M (in-plane direction) and Γ-A (***c*** direction) high-symmetry *k*-path under different strains: (e) w/o strain, (f) 3% compressive uniaxial strain along the *x* axis, (g) 3% compressive uniaxial strain along the *z* axis, and (h) 8% tensile biaxial strain along the in-plane direction. Insets in (f) and (h) illustrate the atomic shift corresponding to the compressive uniaxial and tensile biaxial strains, respectively. Effective masses of holes along the ***c*** direction ($m_{||}$) and along the in-plane ***a*** direction ($m_⊥$) are indicated at the Γ point. The amount of top valence band shift is also indicated. The atomic orbital contribution from N-p_x, p_y, and p_z to each band is also indicated.

dominated by the N-*p* orbital. The atomic orbital origin for each band is illustrated using the molecular orbital diagram: Ga-*s* and N-*p* atomic orbitals interact with each other forming the bonding state and antibonding state, which later become a valence band and conduction band. In unstrained wz-GaN, there are three valence subbands near the Γ point. Traditionally, the two top-most subbands are called the heavy hole (HH) band and light hole (LH) band. A third band (SH), separated by ~30 meV from the other two top-most bands, is due to the crystal-field splitting. The atomic orbital resolved band structure in Fig. 1(d) shows that the two top-most bands are contributed from N-p_x and N-p_y orbitals, while the crystal-field split-off hole band is dominated by the N-p_z orbital.

In Fig. 1(d), due to the in-plane hexagonal symmetry, the p_x and p_y orbital bands are degenerate along the Γ-A (direction parallel to the z axis and $\boldsymbol{c}$ lattice vector) k-path. The other k-path Γ-M (direction parallel to the x axis and $\boldsymbol{a}$ lattice vector) shows the degenerate-lift p_x/p_y band dispersion. Using the parabolic approximation, the calculated hole effective mass along the z axis is $m_{||} = 2.26\, m_0$ and along x axis $m_{\perp} = 1.36\, m_0$, in comparison with the electron effective mass at the conduction band $m_{e,||} = 0.195$ and $m_{e,\perp} = 0.176\, m_0$. These values are in good agreement with experiment data and other reference works.[37,38] Such a large difference in the effective mass corresponds to the large polarity of the carrier mobility between the valence band and the conduction band: the experimentally determined mobility for the electron and hole are 1000and 200 cm^2/V s, respectively.

When strain applied, the atomic orbital overlap interaction will be altered due to the atomic bonding distance change, and as a result, the band dispersion and band structure will be modified. Figures 1(e)–1(h) present the band structure feature at band edges under various biaxial strain and uniaxial strain. It can be seen from Fig. 1(f) that when a compressive strain is applied along the x axis $[(a - a_0)/a_0 = -3\%]$, the p_x orbital band gets pushed up by 0.20 eV in energy. The p_x orbital band dispersion along the x axis becomes significantly stronger characterized by a much smaller effective mass $m_{\perp} = 0.19\, m_0$. Similarly, when a compressive strain applied along the z axis $[(c - c_0)/c_0 = -3\%]$ [Fig. 1(g)], the p_z orbital band is raised up above the p_x/p_y bands (~0.15 eV) with a significantly reduced effective mass along the $\boldsymbol{c}$ axis $m_{||} = 0.18\, m_0$. The results indicate that compressive strain on wz-GaN can raise up the top valence band energy position and decrease the hole effective mass. This would be beneficial for engineering the hole dopability and hole mobility for achieving p-type GaN. Reversely, if we apply a tensile strain, the corresponding band would be pushed down. In Fig. 1(h), the p_x/p_y bands get lowered down below the p_z band when a biaxial tensile strain $[(a - a_0)/a_0 = 8\%,\ (b - b_0)/b_0 = 8\%]$ is applied. This effect results in a reduced effective mass at the top valence band due to the stronger band dispersion of p_z orbital along the z axis.

For p-type semiconductors, the p-type dopability, i.e., the maximum achievable hole concentration, is another critical figure of merit. For GaN and other compound semiconductors, the generally high ionization energy of the acceptor and low solubility lead to hole doping issues. The most widely investigated p-type dopant Mg for GaN presents a high activation energy level above the VBE and high substituting formation energy.[39] The effective mass model predicts that the ionization energy of a dopant can be approximated by $E_a = m^* e^4/8\epsilon^2 h^2$ (13.6 meV).[40] According to this model, heavier effective mass of holes at the valence band would lead to high activation energies of p-type dopants. Recent works on p-type dopability revealed a general trend on the p-type dopability from intrinsic defects point of view: materials with deeper valence band edge tend to be more difficult to be p-type doped because of the spontaneous formation of hole-compensating anion vacancies. In addition to intrinsic hole-compensating defects, acceptor ionization energy is another factor that limits the p-type dopability in wide bandgap semiconductors with deep VBE energy position. Assuming that the acceptor defect energy level is approximately constant in terms of absolute energy scale, which is a reasonable assumption,[41] materials with deep VBE will have high ionization energy of acceptors. If for some reason (e.g., strain) the VBE of the host material shifts up, while the acceptor absolute energy level remains unchanged, this p-type dopant becomes a shallower acceptor due to the reduced activation energy. In Fig. 2(a), we illustrate this idea. The strain effect analysis in the previous part indicates that compressive strain on GaN can raise up the valence band edge, suggesting that strained GaN could achieve low-ionization p-type doping.

To verify this idea, we have performed a detailed defect calculation on various acceptors in GaN to access their defect levels. Group II elements Be, Mg, Ca, and group IIB element Zn are considered. In the defect formation energy plot, it is understood that the Fermi level where the charge transition 0/−1 occurs corresponds to the ionization energy. In Fig. 2(c), for unstrained GaN, Mg presents a relatively large ionization energy of around 209 meV, which is difficult to be activated by the thermal energy at room temperature. While Be exhibits comparatively lower activation energy ~153 meV, its small atomic size means that it prefers occupying the interstitial sites over the substitutional Ga site, which will induce an electron doping effect.[42] The calculated formation energy and ionization energy are in fair agreement with previously experimentally determined data and the theoretically calculated values.[42] Ca and Zn show even higher ionization energies in GaN. Interestingly, when the compressive strain is applied to wz-GaN along the x axis, the ionization energy for Mg in GaN decreases to 40 meV, a significant reduction comparing to unstrained GaN and comparable to typical shallow dopants in conventional semiconductors. The activation energy for shallow acceptor Be even becomes negative, which suggests that it would be spontaneously ionized in strained GaN. The decrease in the ionization energy for acceptors Mg and Be is the result of upshifting of the VBE under the compressive strain as illustrated in Fig. 2(b). In fact, the amount of ionization energy reduction for Mg in GaN (~170 meV) is close to the amount of VBE energy position upshifting (~200 meV). This suggests that the defect level of Mg in GaN is approximately constant and its ionization energy can be rationally modulated by VBE energy position engineering. Compressive strains along other directions also lead to the lowering of Mg and Be ionization energy, as can be seen in Fig. 2(c). The results on the defect levels of Mg and Be in unstrained and strained GaN are summarized in Fig. 2(b).

B. Valence band strain engineering for high-mobility and hole-dopable *p*-type semiconductors

The GaN band structure modulation capability by strain has its fundamental origin. From a molecular orbital point of view, when Ga ($4s^2 4p^1$) and N ($2s^2 2p^3$) atoms join together forming the GaN solid, Ga-4 s/4p and N-2p orbitals interact and form a bonding state and an antibonding state [see Fig. 1(c)]. The bonding state, largely contributed by the N-2p orbital, will be occupied by electrons from both atoms, while the higher energy antibonding state, mostly contributed by the Ga-4 s/4p orbital, remains empty. This is equivalent to the statement that in a GaN crystal, the Ga atom has lost its three 4 s/4p electrons to nitrogen and exhibits the +3 oxidation state. The modern band theory states[43] that the medium-range inter-GaN cell interaction, that is, Ga-4s/Ga-4s orbital interaction, splits the antibonding molecular level into an

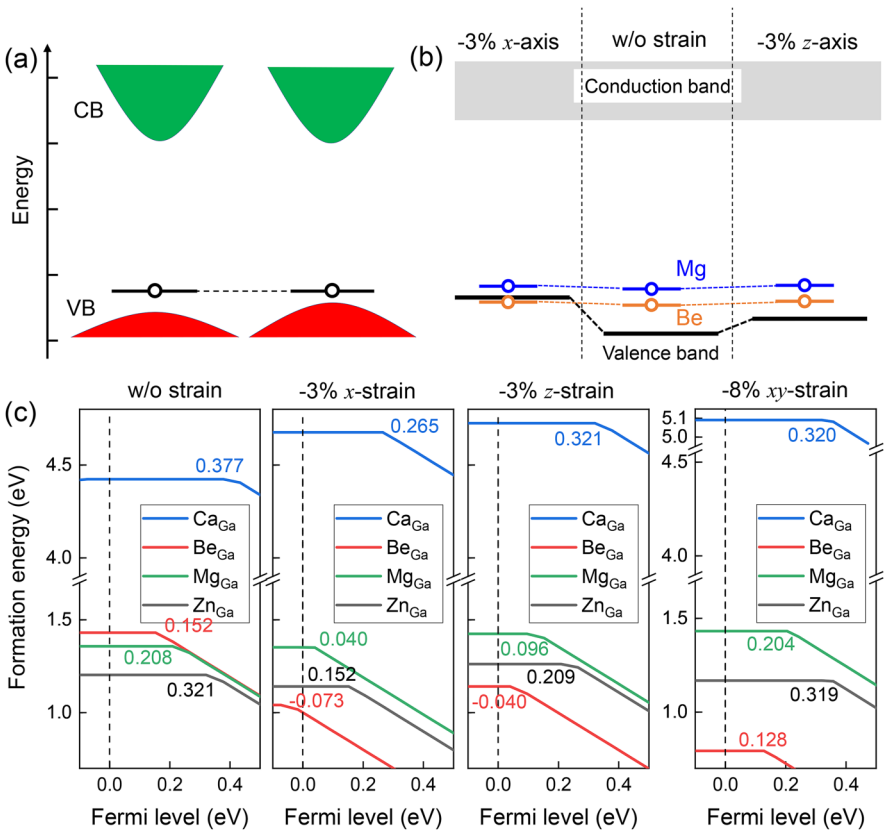

FIG. 2. (a) Schematic showing how the VBE position affects the acceptor defect level. If the acceptor defect energy level is approximately constant in the absolute energy scale, the host material with shallower VBE position will give a shallower acceptor defect level, leading to higher ionization efficiency. (b) Schematics showing how the upshift of the VBE in GaN by strain can modulate the acceptor energy levels of *p*-type dopants Mg and Be. The ionization energies of Be and Mg are approximately constant under strain effect; when the VBE is raised up, their acceptor energies reduce such that they become shallow acceptors. (c) Formation energies of *p*-type dopants in GaN under various strains vs Fermi energy. The zero of the Fermi energy is aligned to the VBE (indicated by the vertical dashed line). The *p*-type dopant activation energies (0/−1 charger transition levels) are indicated in units of eV.

energy band, which comprises the bottom conduction band of GaN (Ga-4*p*/Ga-4*p* orbital interaction also splits the antibonding molecular level into another energy band, which is higher than the bottom Ga-4*s* dominated conduction band), while the orbital interaction between N-2*p*/-2*p* causes the bonding molecular level to split into the top valence band of GaN. The energy level difference between the bonding and antibonding states would determine the GaN bandgap. The energy band disperses up and down depending on the orbital in-phase (bonding) or out-of-phase (antibonding) interaction and centers at the molecular orbital energy level (see Fig. 3). For GaN, the N-2*p* orbital dominated top valence band is centered at the N-2*p* bonding state energy level; therefore, the absolute energy level of the top valence band is deep since the N-2*p* atomic orbital is deep relative to the vacuum level. The top valence band dispersion is due to the medium-range inter-unit cell N-2*p*/N-2*p* atomic orbital overlap interaction (and possibly also due to the short-range inner-unit cell N-2*p*/Ga-4 *s*/N-2*p* indirect orbital overlap interaction). When a compressive strain being applied, the interatomic distance decreases, leading to a stronger interatomic orbital interaction, and as a result, the band dispersion becomes stronger. This increased top valence band dispersion due to decreased N–N (and N–Ga–N) interatomic distance will result in the upshift of the valence band edge, narrowing of bandgap, and reduction in the hole effective mass at the VBE. This explains why compressive strain in GaN could raise the energy position of VBE and reduce the effective mass of holes at VBE.

The valence band modulation ability including energy position upshifting and hole mobility enhancing relies on the top valence band orbital character, i.e., the top valence band states are dominated by anion's *p* orbitals. Therefore, the strain engineering to enhance

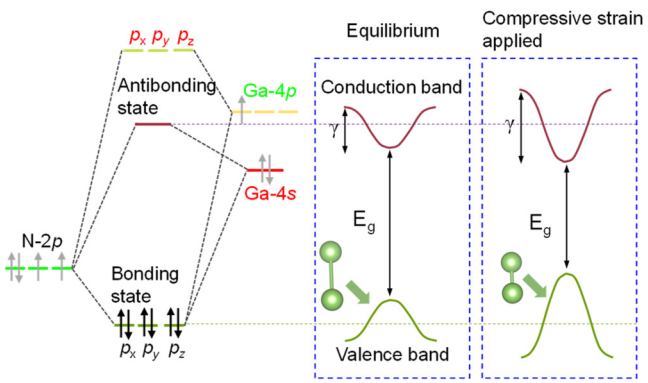

FIG. 3. Schematics showing how strain modifies the band dispersion structure in GaN from a molecular orbital point of view. A compressive strain decreases the interatomic distance and increases interatomic orbital overlap interaction strength. As a result, the band dispersion due to the atomic orbital overlap interaction becomes stronger, leading to a widened band width (γ), narrowed bandgap (E_g), and reduced band effective mass.

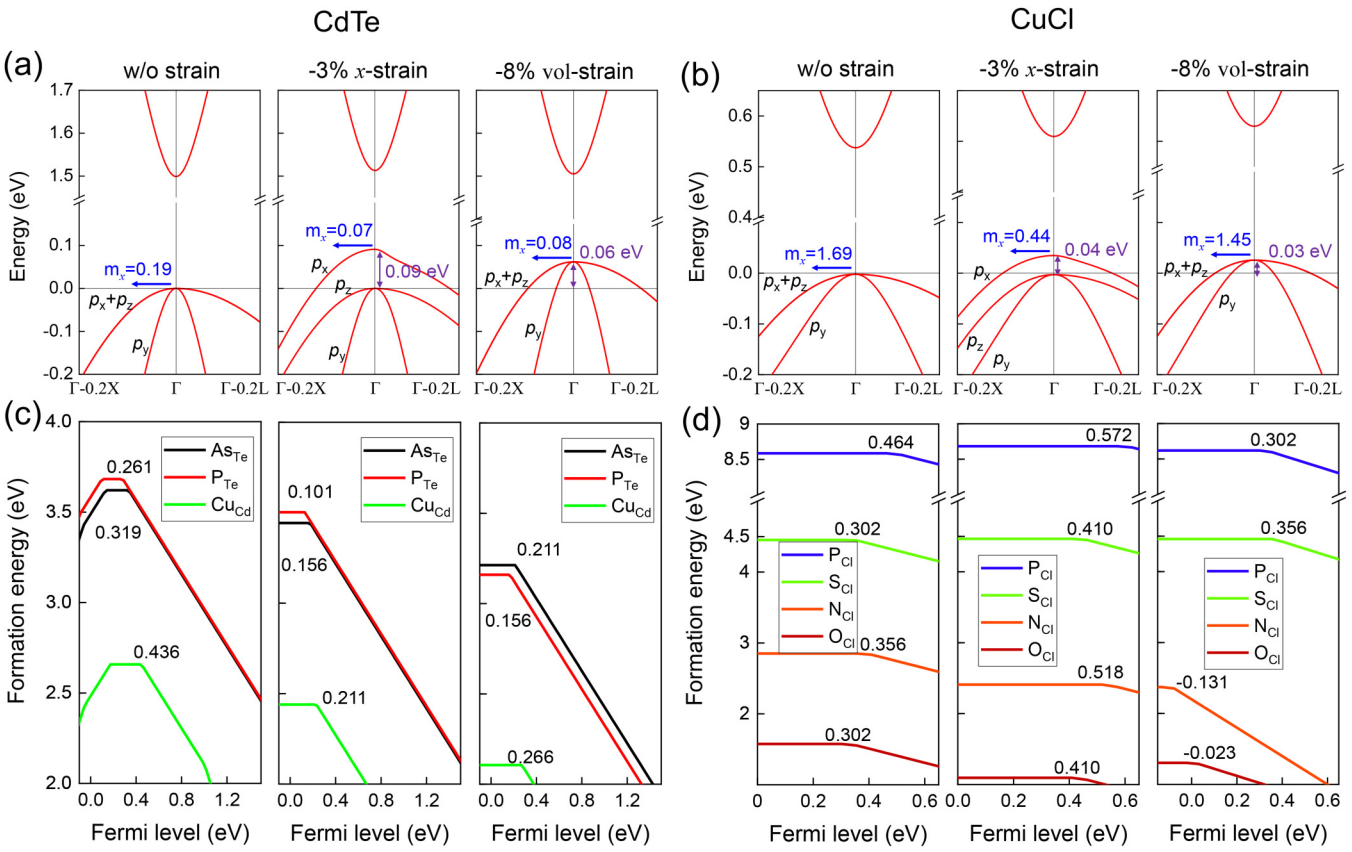

FIG. 4. (a) and (b) Valence band structure details of (a) CdTe and (b) CuCl along Γ-X (*x*-axis direction) and Γ-L (body-diagonal direction) high-symmetry *k*-path under different strains: w/o strain, 3% compressive uniaxial strain along the *x* axis, and 8% compressive volumetric strain. Effective masses of hole along the ***x*** direction (m_x) are indicated at the Γ point. The amount of top valence band shift is also indicated. The atomic orbital contribution from anion-p_x, p_y, and p_z to each band is also indicated. (c) and (d) Formation energies of *p*-type dopants in (c) CdTe and (d) CuCl under various strains vs Fermi energy. The zero of the Fermi energy is aligned to the VBE. The *p*-type dopant activation energies (0/−1 charger transition levels) are indicated in units of eV.

the *p*-type dopability (i.e., raising up the VBE energy position) and hole mobility (reducing the hole effective mass) could be generally extended to other compound semiconductors such as nitrides-, oxides-, chalcogenides-, halides-, and mixed-anions-based semiconductors, as these compounds have their VBE states mainly derived from anion's *p* orbitals. To examine this idea, in Secs. III C–III G, we apply strain engineering to a broad class of compound semiconductors including chalcogenides, halides, transition metal oxides, post-transition metal oxides, and mixed-anions metal oxides. We will show that strain engineering can be universally applicable to a wide range of compound semiconductors for high hole mobility and *p*-type dopability.

C. Chalcogenides and halides: CdTe and CuCl

We first consider chalcogenides and halides. Figures 4(a) and 4(b) show the calculated valence band structures of CdTe (chalcogenide) and CuCl (halide). There are ongoing studies on improving the *p*-type doping performance of CdTe as a photovoltaic material[44–48] and CuCl as the UV-range optoelectronic material.[49,50] For chalcogenide CdTe, with a compressive uniaxial strain applied along the *x* axis, the p_x-derived band gets pushed up and moves above the p_y and p_z bands by ∼0.09 eV. When applied a volumetric compressive strain, all p_x, p_y, and p_z derived bands move up. The compressive strain along the *x*-axis direction and the volumetric strain also result in a decreased effective hole mass at the top valence band, from ∼0.19 m_0 to 0.07 and 0.08 m_0, respectively. Similarly, for halide CuCl, both the uniaxial strain and volumetric strain could lead to upshifted valence band upshift and decreased hole effective mass. The amount of the valence band edge shift and hole effective mass change are summarized in Fig. 4(b). It is expected that the upraised valence band would result in enhanced *p*-type dopability, i.e., reduced acceptor ionization energy. Figures 4(c) and 4(d) present the defect formation energy in CdTe and CuCl showing their defect charge transition levels. The *p*-type dopants in CdTe and CuCl exhibit shallower charge transition levels with strain applied. In CdTe, the *p*-type dopants As_{Te}, P_{Te}, and Cu_{Cd} exhibit a shallower 0/−1 charge transition level when strain applied, meaning that these dopants can be easily ionized in stained

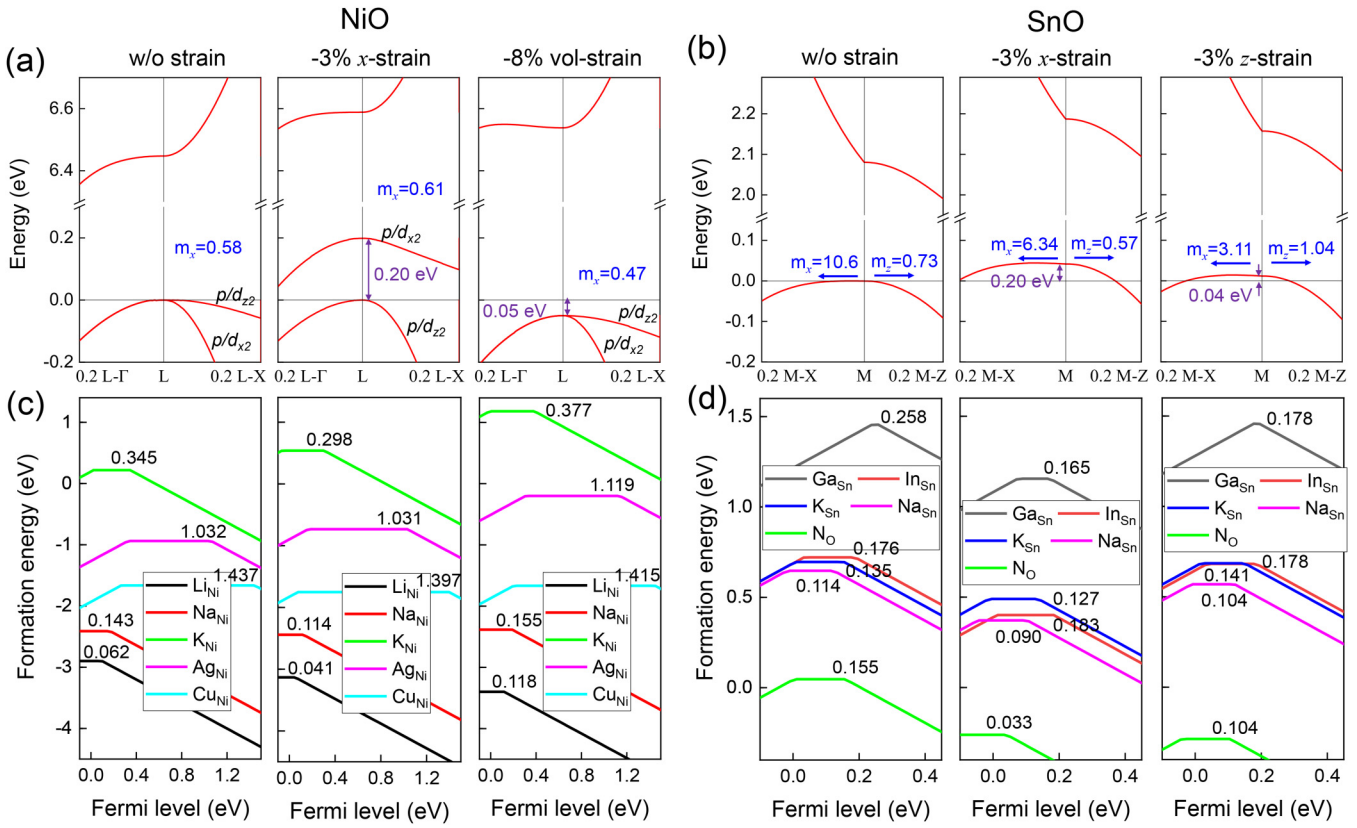

FIG. 5. (a) Valence band structure details of NiO along the L-Γ (body-diagonal direction) and Γ-X (face-diagonal direction) high-symmetry *k*-path under different strains: w/o strain, 3% compressive uniaxial strain along the *x* axis, and 8% compressive volumetric strain. Effective masses of holes along the ***x*** direction (m_x) are presented. The atomic orbital contribution from Ni d_x^2 and d_z^2, and O-*p* to each band is also indicated. (b) Valence band structure details of SnO along the M-X (*x*-axis direction) and M-Z (*z*-axis direction) high-symmetry *k*-path under different strains: w/o strain, and 3% compressive uniaxial strain along the *x* axis, and 3% compressive uniaxial strain along *z* axis. Effective masses of holes along the ***x*** direction (m_x) and along ***z*** direction (m_z) are indicated at the M point. (c) and (d) Formation energies of *p*-type dopants in (c) NiO and (d) SnO under various strains vs Fermi energy. The zero of the Fermi energy is aligned to the VBE. The *p*-type dopant activation energies (0/−1 charger transition levels) are indicated in units of eV.

CdTe. A similar trend also happens in CuCl. For both CdTe and CuCl, uniaxial strain is more effective than volumetric strain in decreasing the acceptor ionization energies. The results on CdTe and CuCl suggest that strain engineering can be applied to chalcogenides and halides for enhanced *p*-type dopability and hole mobility.

D. Transition metal-based oxides: NiO

p-type transition metal oxides rely on their high *p*-type oxide performance on the hybridization of transition metals' *d*-orbitals with oxygen's *p* orbitals at the valence band edge. This alleviates the dominance of oxygen *p*-orbitals at the top valence band for achieving dispersive valence band with small hole effective mass and high hole dopability with shallow valence band edge.[51,52] Transition metals that could be employed to design high-mobility and hole-dopable *p*-type oxides include Cu (Cu_2O)[53] and Ni (NiO).[54]. Since lattice strain engineering applies to anion's *p* orbitals based valence bands, it is worthwhile to investigate whether strain engineering is also applicable to transition metals' *d*-orbital based valence bands. Here, we performed a detailed band structure and defect calculation on NiO under strain conditions. For rock salt type NiO, its valence band edge states are contributed from Ni-3*d* and O-2*p* orbitals. A full band structure of NiO is shown in Fig. S1 in the supplementary material. The involvement of extended Ni-3*d* orbitals at the VBE results in a relatively dispersive and shallow valence band, giving rise to the possibility of application as a *p*-type oxide. In Fig. 5(a), the VBM is located at the *L* point with the top two degenerate valence bands overlapping with each other. Under uniaxial compressive strain along the *x* axis, the d_{xz}/O-*p* orbital derived band gets pushed up and shifts above the d_{yz}/O-*p* orbital band. This behavior is like *s*-*p*-type compounds where p_x bands can be modulated upshift by strain along the *x* axis. The hole effective mass at the VBE also decreases, resulting in increased hole mobility. Following this, we have calculated the defect formation energy to access the ionization energy of *p*-type dopants in NiO. There are various acceptor candidates for NiO in the literature, including Cu, Ag, Li, Na, K, Rb, and

Cs to substitute for Ni,[55] and N, P, and As to substitute for O. In our calculation, a selected group of *p*-type dopants, Li, Na, K, Ag, and Cu, were examined. Figure 5(c) presents the defect formation energies of these *p*-type dopants. Under an equilibrium state without strain applied, acceptors Li, Na, and K all exhibit shallow ionization energy levels, i.e., their 0/−1 charge transition levels located close to the VBE. When compressive strain applied along the *x*-axis direction, their 0/−1 charge transition levels move even closer to the VBE, leading to further reduced activation energies. The reduced ionization energy would enhance the acceptors' activation and increase the maximum achievable hole concentration. It is observed that in NiO, the volumetric strain does not effectively decrease the ionization energy levels of *p*-type dopants and is not capable of increasing the hole dopability in NiO.

E. Post-transition metal oxides: SnO

Post-transition metal oxides originate their *p*-type conductivity from the hybridization of post-transition metals' *s*-orbitals with oxygen *p* orbitals. Like *p*-type transition metal oxides, the overlapping of extended metals' *s* orbitals with O-*p* orbitals could alleviate the localization of the valence bands. Post-transition metals that have been studied or proposed to design high-mobility and hole-dopable *p*-type oxides include Sn(SnO), Bi(Bi_2O_3), Pb(PbO), Tl(Tl_2O), and Sb(Sb_2O_3).[2,6,33,56–60] To test whether strain engineering is also applicable to modulate the post-transition metals' *s* orbital based valence bands, We have performed a detailed band structure and defect calculation on SnO under strain conditions. A full band structure of tetragonal phase layer structured SnO is presented in Fig. S2 in the supplementary material. At the top valence bands, there is a large presence of Sn-5*s* orbital hybridizing with O-*p* orbitals. This results in the dispersive valence band and shallow valence band edge energy position. Figure 5(b) shows that with a compressive strain applied along the in-plane *x* direction and out-of-plane *z* direction, the VBE shifts up, suggesting a shallower valence band and higher *p*-type doping capability. The valence band dispersion, quantized by hole effective mass, is indicated in Fig. 5(b), which shows lighter holes when strain applied. This points to a higher hole mobility for strained SnO. We have calculated the activation energies for possible *p*-type dopants in SnO, including Ga, In, K, and Na substituting for Sn, and N substituting for O. From Fig. 5(d), it can be seen that both *x* axis and *z* axis strain can push the 0/−1 charge transition level closer to the valence band, pointing to a lower activation energy. Both increased hole mobility and decreased *p*-dopants' activation energy will enhance the *p*-type oxide performance of SnO.

F. Mixed anion metal oxides: ZrOS

Oxides with mixed anions are another group of *p*-type oxides that have been identified for potentially transparent conducting oxide (TCO) candidates. Oxychalcogenides, such as ZrOS and LaCuOS, and oxyhalides, such as $Sb4Cl_2O_5$, have been reported as high-mobility transparent oxides.[2,61–63] The contribution of non-oxygen anions to valence band states would alleviate the dominance of oxygen *p* orbital. Owing to the spatially more extended, higher energy of the *p*-orbitals from these non-oxygen elements (chalcogens, for example), their valence bands are more dispersive and shallow-lying, allowing for high hole mobility and good *p*-type dopability. As *p*-type oxide candidates, oxychalcogenides or oxypnictogen are worthwhile to investigate whether strain engineering can boost their hole mobility and dopability. Here, we focus ZrOS as such kind of *p*-type semiconductor and investigate the modulating effect of lattice strain on its *p*-type semiconductor performance. The calculated full band structure of ZrOS (Fig. S3 in the supplementary material) shows that the valence band is dominated by O-2*p* orbitals and S-3*p* orbitals. In Fig. 6(a), under compressive strain along the *x* axis, the S-p_x orbital derived band shifts up and moves above the S-p_z band by 0.14 eV. Meanwhile, the S-p_y band moved down by 0.04 eV. The effective mass of holes at the top valence band along the *x* axis decreases from 2.84 m_0 to 0.35 m_0. *p*-type dopant activation energy calculation was performed, proving that a 3% compressive strain along the *x*- axis direction is effective in lowering the *p*-dopant ionization energies, as those defects [Cu_{Zr}, N_O, for example, in Fig. 6(c)] exhibit a 0/−1 charge transition level closer to the valence band. Volumetric strain was also examined, and it is found that the volumetric strain is not as effective as uniaxial strain in raising up the valence band and lowering the *p*-dopant activation energy. The about results indicate that strain engineering can be applied to mixed-anions-based oxides for enhanced *p*-type dopability and hole mobility.

G. Normally *n*-type oxides: SnO_2, ZnO, Ga_2O_3, and In_2O_3

There are attempts to *p*-dope widely used *n*-type oxides, for example, ZnO.[64–67] It is natural to extend the strain engineering to those normally *n*-type oxides. Currently, oxide semiconductors with *n*-type conduction, such as SnO_2, ZnO, and In_2O_3, are commercially available with high electron mobility and controllable carrier concentrations. In contrast, very few *p*-type oxide semiconductors have been developed until now, due to the deep-lying and spatially localized O-2*p* orbitals dominating at the VBM limiting their hole mobilities and hole dopability. Given the context, applying strain to raising up the VBM position and to engineer the band dispersion in oxides would be a potential way to develop high-mobility and hole-dopable *p*-type oxides. In this work, we have studied the strain effect on ZnO, which has been investigated as a possible *p*-type transparent conducting oxide.[64–67] Figure 6(b) shows the calculated valence band structures of ZnO under various strain conditions. For *n*-type oxide ZnO, both uniaxial strain and volumetric strain lead to an upshift of the top valence bands and the reduction in hole effective masses. However, in ZnO, two *p*-type dopant candidates, Ag substituting for Zn (Ag_{Zn}) and N substituting for O (N_O), do not show significantly decreased ionization energy [Fig. 6(d)]. Ag_{Zn} and N_O exhibit a deep charge transition level in both the unstrained and strained ZnO. This suggests that strain engineering is not effective in enhancing the *p*-type dopability in ZnO. A possible explanation is that in oxides where the top valence band is dominated by oxygen *p* orbitals, O-*p* orbitals are highly localized and very deep in the energy position such that strain cannot effectively bring up the O-*p* orbital derived valance band to a shallow level. This is supported by the observation that while the valence band edge has shifted after compressive strain, the amount of upshift is only ~0.1 eV, which can hardly compensate the deep-lying oxygen *p* orbital bands in oxides for higher

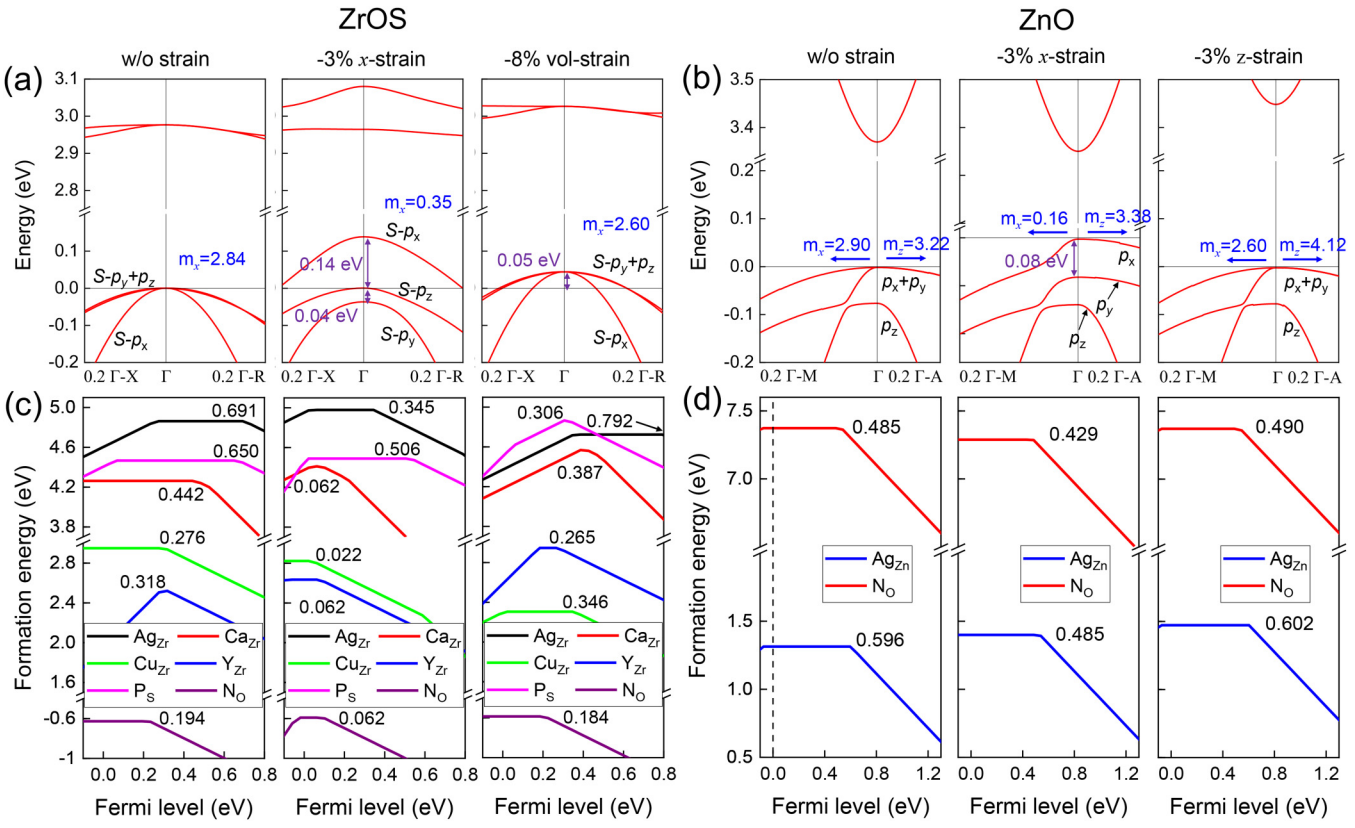

FIG. 6. (a) Valence band structure details of ZrOS along the L-X (*x*-axis direction) and Γ-R (body-diagonal direction) high-symmetry *k*-path under different strains: w/o strain, 3% compressive uniaxial strain along the *x* axis, and 8% compressive volumetric strain. Effective masses of holes along the ***x*** direction (m_x) are presented. The atomic orbital contribution from S-p_x, p_y, p_z to each band is also indicated. (b) Valence band structure details of ZnO along the Γ-M (*x*-axis direction) and Γ-A (*z*-axis direction) high-symmetry *k*-path under different strains: w/o strain, and 3% compressive uniaxial strain along the *x* axis, and 3% compressive uniaxial strain along the *z* axis. Effective masses of holes along the ***x*** direction (m_x) and along the ***z*** direction (m_z) are indicated at the Γ point. The atomic orbital contribution from S-p_x, p_y, p_z to each band is also indicated. (c) and (d) Formation energies of *p*-type dopants in (c) ZrOS and (d) ZnO under various strains vs Fermi energy. The zero of the Fermi energy is aligned to the VBE. The *p*-type dopant activation energies (0/−1 charger transition levels) are indicated in units of eV.

dopability. We have also examined other oxides including SnO_2 and Ga_2O_3, which also show a negligible effect of the strain engineering on the modulation of the *p*-dopants activation energies (see Figs. S4 and S5 in the supplementary material). The results suggest that in oxides, the O-2*p* dominated VBM is insensitive to the lattice strain and strain engineering is not applicable to such group of oxides for high performance *p*-type oxide development.

H. Discussion

Previous works on *p*-type dopability pointed out a general trend on the *p*-type dopability from intrinsic defects point of view: materials with deeper valence band edge tend to be more difficult to be *p*-type doped because of the spontaneous formation of the hole-compensating anion vacancies. The transition points of the spontaneous formation of anion vacancy define the "Fermi level doping range," which is the maximum Fermi level modulating range by doping without inducing compensating defects' spontaneous formation. The Fermi level doping range across different materials does not significantly vary such that the different materials can be compared against each other on a common absolute energy scale. Materials with shallower VBE position would have higher hole dopability. Engineering the VBE position is an efficient way to enhance the *p*-type semiconductor performance for compound semiconductors.

Compound semiconductors typically consist of metal cations and non-metal anions. The common feature among these compounds is that their valence band edges are the antibonding states of cations' and anions' orbitals. When compressive strain is applied onto these compounds, the interatomic distance decreases, leading to a strengthened orbital overlap interaction. As a result, from a tight binding point of view, the top valence band will have a stronger dispersion. This has two consequences: first, the hole effective mass at the top valence band reduces; second, the valence band edge energy level shifts up. Our calculations in this work show that *s*-*p*-type compounds, post-transition metal *p*-type oxides (metal's *s* type compounds), transition metal *p*-type oxides (metal's *d* type

compounds), and mixed-anions compounds all show the valance band mouldability by strain engineering. The valence band modulation ability including VBM energy level upshifting and hole mobility enhancing relies on the top valence band orbital character, i.e., the top valence band states are dominated by anion's *p* orbitals. Therefore, the strain engineering to enhance the *p*-type dopability (i.e., raising up the VBE energy position) and hole mobility (reducing hole effective mass) could generally apply to compound semiconductors, as these compounds have their VBE states mainly derived from anion's *p*-orbitals.

Our calculation results also show that the *p*-dopant activation energy level in a material is almost constant in the absolute energy scale. This is also consistent with the previous literature report.[41] Therefore, materials with shallower VBE position will have their *p*-dopants easier to be activated since the activation energy level is located closer to valence band. Engineering the materials to shift up the VBE would reduce the activation energy of *p*-type dopants, resulting in a higher *p*-type doping performance.

Our calculation proves that, except for normally *n*-type oxides, other compound semiconductors including nitrides, chalcogenides, transition metal oxides, post-transition metal oxides, and mixed-anions compounds are very promising for strain engineering to modulate the hole mobility and *p*-type dopability. This provides a viable way to enhance the *p*-type semiconductor performance by strain engineering. Experimentalists are recommended to incorporate strain process into materials synthesis and processing to achieve better performed *p*-type semiconductors in various semiconductor devices.

IV. CONCLUSION

In conclusion, we have performed DFT-based first-principles calculations to investigate the strain effect on the band structures and *p*-dopants activation energies of compounds in terms of *p*-type semiconductor application. Compressive lattice strain can generally lead to top valence band upshifting and hole effective mass decreasing in compound semiconductors, which can be exploited to enhance the hole mobility and *p*-type dopability for those compounds as *p*-type semiconductors. A wide range of compounds including nitrides, chalcogenides, halides, post-transition metal oxides, transition metal oxides, and mixed-anion based oxides are very promising in terms of strain engineering for better performed *p*-type semiconductors. This work demonstrates that strain engineering can be universal to enhance *p*-type performance. Our work also suggests a viable way to achieve high performance *p*-type semiconductors by strain engineering.

SUPPLEMENTARY MATERIAL

See the supplementary material for the crystal structure and band structure of NiO, crystal structure and band structure of SnO, crystal structure and band structure of ZrOS, formation energies of p-type dopants in SnO_2, and formation energies of p-type dopants in Ga_2O_3.

AUTHOR DECLARATIONS

Conflict of Interest

The authors have no conflicts to disclose.

Author Contributions

Yaoqiao Hu: Conceptualization (lead); Data curation (lead); Formal analysis (lead); Methodology (lead); Validation (lead); Visualization (lead); Writing – original draft (lead); Writing – review & editing (lead). **Kyeongjae Cho:** Funding acquisition (lead); Investigation (lead); Project administration (lead); Resources (lead); Supervision (lead); Writing – original draft (supporting); Writing – review & editing (supporting).

DATA AVAILABILITY

The data that support the findings of this study are available within the article and its supplementary material.

REFERENCES

[1]H. Amano, Y. Baines, E. Beam, M. Borga, T. Bouchet, P. R. Chalker, M. Charles, K. J. Chen, N. Chowdhury, and R. Chu, "The 2018 GaN power electronics roadmap," J. Phys. D: Appl. Phys. **51**(16), 163001 (2018).
[2]G. Hautier, A. Miglio, G. Ceder, G.-M. Rignanese, and X. Gonze, "Identification and design principles of low hole effective mass p-type transparent conducting oxides," Nat. Commun. **4**(1), 2292 (2013).
[3]S. Brochen, J. Brault, S. Chenot, A. Dussaigne, M. Leroux, and B. Damilano, "Dependence of the Mg-related acceptor ionization energy with the acceptor concentration in p-type GaN layers grown by molecular beam epitaxy," Appl. Phys. Lett. **103**(3), 032102 (2013).
[4]T. Narita, H. Yoshida, K. Tomita, K. Kataoka, H. Sakurai, M. Horita, M. Bockowski, N. Ikarashi, J. Suda, and T. Kachi, "Progress on and challenges of p-type formation for GaN power devices," J. Appl. Phys. **128**(9), 090901 (2020).
[5]J. Robertson and S. Clark, "Limits to doping in oxides," Phys. Rev. B **83**(7), 075205 (2011).
[6]Y. Hu, X. Yao, D. G. Schlom, S. Datta, and K. Cho, "First principles design of high hole mobility p-type Sn–O–X ternary oxides: Valence orbital engineering of Sn^{2+} in Sn^{2+}–O–X by selection of appropriate elements X," Chem. Mater. **33**(1), 212–225 (2020).
[7]A. Zunger, "Practical doping principles," Appl. Phys. Lett. **83**(1), 57–59 (2003).
[8]M. Chu, Y. Sun, U. Aghoram, and S. E. Thompson, "Strain: A solution for higher carrier mobility in nanoscale MOSFETs," Annu. Rev. Mater. Res. **39**, 203–229 (2009).
[9]A. Chaves, J. G. Azadani, H. Alsalman, D. Da Costa, R. Frisenda, A. Chaves, S. H. Song, Y. D. Kim, D. He, and J. Zhou, "Bandgap engineering of two-dimensional semiconductor materials," npj 2D Mater. Appl. **4**(1), 29 (2020).
[10]Z. Peng, X. Chen, Y. Fan, D. J. Srolovitz, and D. Lei, "Strain engineering of 2D semiconductors and graphene: From strain fields to band-structure tuning and photonic applications," Light: Sci. Appl. **9**(1), 190 (2020).
[11]G. Gui, J. Li, and J. Zhong, "Band structure engineering of graphene by strain: First-principles calculations," Phys. Rev. B **78**(7), 075435 (2008).
[12]H. Wang, Y.-S. Lan, B. Dai, X.-W. Zhang, Z.-G. Wang, and N.-N. Ge, "Improved thermoelectric performance of monolayer HfS_2 by strain engineering," ACS Omega **6**(44), 29820–29829 (2021).
[13]C.-W. Wu, X. Ren, G. Xie, W.-X. Zhou, G. Zhang, and K.-Q. Chen, "Enhanced high-temperature thermoelectric performance by strain engineering in BiOCl," Phys. Rev. Appl. **18**(1), 014053 (2022).
[14]D. Guo, C. Li, K. Li, B. Shao, D. Chen, Y. Ma, J. Sun, X. Cao, W. Zeng, and R. Yang, "The strain-induced excellent thermoelectric performance of PbTe," Physica E **130**, 114685 (2021).
[15]S.-D. Guo, "Biaxial strain tuned thermoelectric properties in monolayer $PtSe_2$," J. Mater. Chem. C **4**(39), 9366–9374 (2016).
[16]J. Xiang, H. Wang, B. Dai, W.-L. Cheng, X.-W. Zhang, Z.-G. Wang, and N.-N. Ge, "Optimizing the thermoelectric transmission of monolayer $HfSe_2$ by strain engineering," J. Phys. Chem. Solids **169**, 110834 (2022).

[17]J. Zhao, H. Zeng, and X. Zhou, "X_3n (X=C and Si) monolayers and their van der Waals heterostructures with graphene and h-BN: Emerging tunable electronic structures by strain engineering," Carbon **145**, 1–9 (2019).
[18]Y. Miao, H. Bao, W. Fan, and F. Ma, "Modulation of the electronic structure and magnetism performance of V-doped monolayer MoS_2 by strain engineering," J. Phys. Chem. Solids **142**, 109459 (2020).
[19]Z. Deng and X. Wang, "Strain engineering on the electronic states of two-dimensional GaN/graphene heterostructure," RSC Adv. **9**(45), 26024–26029 (2019).
[20]B. Zeng, M. Long, X. Zhang, Y. Dong, M. Li, Y. Yi, and H. Duan, "Strain engineering on electronic structure and carrier mobility in monolayer GeP_3," J. Phys. D: Appl. Phys. **51**(23), 235302 (2018).
[21]W. Zhou and N. Umezawa, "Viable approach toward efficient p-type conductivity in Al-doped anatase TiO_2 via strain engineering," RSC Adv. **7**(33), 20542–20547 (2017).
[22]X. Li, X. Song, J. Du, W. Xiong, and C. Xia, "Strain-tunable p-type Ag doping in the native n-type InSe monolayer," Appl. Surf. Sci. **462**, 387–392 (2018).
[23]B. Kang, S. Kim, J. Kim, F. Ren, K. Baik, S. Pearton, B. Gila, C. Abernathy, C.-C. Pan, and G.-T. Chen, "Effect of external strain on the conductivity of AlGaN/GaN high-electron-mobility transistors," Appl. Phys. Lett. **83**(23), 4845–4847 (2003).
[24]S. Bae, Y.-G. Kang, K. Ichihashi, M. Khazaei, V. Swamy, M. J. Han, K. J. Chang, K.-i. Shudo, and H. Raebiger, "Strain engineering to release trapped hole carriers in p-type Haeckelite GaN," ACS Appl. Electron. Mater. **3**(12), 5257–5264 (2021).
[25]G. Kresse and J. Hafner, "*Ab initio* molecular dynamics for liquid metals," Phys. Rev. B **47**(1), 558 (1993).
[26]G. Kresse and J. Furthmüller, "Efficient iterative schemes for *ab initio* total-energy calculations using a plane-wave basis set," Phys. Rev. B **54**(16), 11169 (1996).
[27]G. Kresse and J. Hafner, "Norm-conserving and ultrasoft pseudopotentials for first-row and transition elements," J. Phys.: Condens. Matter **6**(40), 8245 (1994).
[28]G. Kresse and D. Joubert, "From ultrasoft pseudopotentials to the projector augmented-wave method," Phys. Rev. B **59**(3), 1758 (1999).
[29]J. P. Perdew, K. Burke, and M. Ernzerhof, "Generalized gradient approximation made simple," Phys. Rev. Lett. **77**(18), 3865 (1996).
[30]H. J. Monkhorst and J. D. Pack, "Special points for Brillouin-zone integrations," Phys. Rev. B **13**(12), 5188 (1976).
[31]M. P. Teter, M. C. Payne, and D. C. Allan, "Solution of Schrödinger's equation for large systems," Phys. Rev. B **40**(18), 12255 (1989).
[32]G. Kresse and J. Furthmüller, "Efficiency of ab-initio total energy calculations for metals and semiconductors using a plane-wave basis set," Comput. Mater. Sci. **6**(1), 15–50 (1996).
[33]Y. Hu, D. Schlom, S. Datta, and K. Cho, "Interlayer engineering of band gap and hole mobility in p-type oxide SnO," ACS Appl. Mater. Interfaces **14**(22), 25670–25679 (2022).
[34]S. Zhang and J. E. Northrup, "Chemical potential dependence of defect formation energies in GaAs: Application to Ga self-diffusion," Phys. Rev. Lett. **67**(17), 2339 (1991).
[35]C. Freysoldt, J. Neugebauer, and C. G. Van de Walle, "Electrostatic interactions between charged defects in supercells," Phys. Status Solidi B **248**(5), 1067–1076 (2011).
[36]D. Broberg, B. Medasani, N. E. Zimmermann, G. Yu, A. Canning, M. Haranczyk, M. Asta, and G. Hautier, "PyCDT: A python toolkit for modeling point defects in semiconductors and insulators," Comput. Phys. Commun. **226**, 165–179 (2018).
[37]S. Poncé, D. Jena, and F. Giustino, "Hole mobility of strained GaN from first principles," Phys. Rev. B **100**(8), 085204 (2019).
[38]See http://www.ioffe.ru/SVA/NSM/Semicond/GaN/ebasic.html for information about the electron effective masses in GaN (last accessed September 2022).
[39]K. Kumakura, T. Makimoto, and N. Kobayashi, "Activation energy and electrical activity of Mg in Mg-doped $In_xGa_{1-x}N$ (x>0.2)," Jpn. J. Appl. Phys. **39**(4B), L337 (2000).
[40]W. Tsang, E. Schubert, and J. Cunningham, "Doping in semiconductors with variable activation energy," Appl. Phys. Lett. **60**(1), 115–117 (1992).
[41]S. Y. Ren, J. D. Dow, and S. Klemm, "Strain-assisted p-type doping of II-VI semiconductors," J. Appl. Phys. **66**(5), 2065–2068 (1989).
[42]H. Ahmad, T. J. Anderson, J. C. Gallagher, E. A. Clinton, Z. Engel, C. M. Matthews, and W. Alan Doolittle, "Beryllium doped semi-insulating GaN without surface accumulation for homoepitaxial high power devices," J. Appl. Phys. **127**(21), 215703 (2020).
[43]C. Kittel and P. McEuen, *Introduction to Solid State Physics* (John Wiley & Sons, 2018).
[44]B. McCandless, W. Buchanan, G. Sriramagiri, C. Thompson, J. Duenow, D. Albin, S. A. Jensen, J. Moseley, M. Al-Jassim, and W. K. Metzger, "Enhanced p-type doping in polycrystalline CdTe films: Deposition and activation," IEEE J. Photovoltaics **9**(3), 912–917 (2019).
[45]J. J. McCoy, S. K. Swain, J. R. Sieber, D. R. Diercks, B. P. Gorman, and K. G. Lynn, "p-type doping efficiency in CdTe: Influence of second phase formation," J. Appl. Phys. **123**(16), 161579 (2018).
[46]A. Nagaoka, D. Kuciauskas, J. McCoy, and M. A. Scarpulla, "High p-type doping, mobility, and photocarrier lifetime in arsenic-doped CdTe single crystals," Appl. Phys. Lett. **112**(19), 192101 (2018).
[47]J.-H. Yang, W.-J. Yin, J.-S. Park, J. Burst, W. K. Metzger, T. Gessert, T. Barnes, and S.-H. Wei, "Enhanced p-type dopability of P and As in CdTe using non-equilibrium thermal processing," J. Appl. Phys. **118**(2), 025102 (2015).
[48]J.-H. Yang, W.-J. Yin, J.-S. Park, J. Ma, and S.-H. Wei, "Review on first-principles study of defect properties of CdTe as a solar cell absorber," Semicond. Sci. Technol. **31**(8), 083002 (2016).
[49]L. O'Reilly, A. Mitra, G. Natarajan, O. Lucas, P. McNally, S. Daniels, D. Cameron, A. Bradley, and A. Reader, "Impact on structural, optical and electrical properties of CuCl by incorporation of Zn for n-type doping," J. Cryst. Growth **287**(1), 139–144 (2006).
[50]D. Huang, J.-P. Xu, J.-W. Jiang, Y.-J. Zhao, B.-L. Peng, W.-Z. Zhou, and J. Guo, "Difficulty of long-standing n-type conductivity in equilibrium and non-equilibrium γ-CuCl: A first-principles study," Phys. Lett. A **381**(33), 2743–2747 (2017).
[51]Z. Wang, P. K. Nayak, J. A. Caraveo-Frescas, and H. N. Alshareef, "Recent developments in p-type oxide semiconductor materials and devices," Adv. Mater. **28**(20), 3831–3892 (2016).
[52]K. H. Zhang, K. Xi, M. G. Blamire, and R. G. Egdell, "P-type transparent conducting oxides," J. Phys.: Condens. Matter **28**(38), 383002 (2016).
[53]H. Kawazoe, M. Yasukawa, H. Hyodo, M. Kurita, H. Yanagi, and H. Hosono, "P-type electrical conduction in transparent thin films of $CuAlO_2$," Nature **389**(6654), 939–942 (1997).
[54]H. Sato, T. Minami, S. Takata, and T. Yamada, "Transparent conducting p-type NiO thin films prepared by magnetron sputtering," Thin Solid Films **236**(1-2), 27–31 (1993).
[55]K. O. Egbo, C. E. Ekuma, C. P. Liu, and K. M. Yu, "Efficient p-type doping of sputter-deposited NiO thin films with Li, Ag, and Cu acceptors," Phys. Rev. Mater. **4**(10), 104603 (2020).
[56]Y. Hu, D. Schlom, S. Datta, and K. Cho, "Amorphous Ta_2SnO_6: A hole-dopable p-type oxide," Appl. Surf. Sci. **613**, 155981 (2023).
[57]Y. Hu, D. Schlom, S. Datta, and K. Cho, "Ilmenite and amorphous $SnTiO_3$ as p-type oxide semiconductors," J. Mater. Chem. C **11**(14), 4830–4836 (2023).
[58]J. Shi, E. A. Rubinstein, W. Li, J. Zhang, Y. Yang, T. L. Lee, C. Qin, P. Yan, J. L. MacManus-Driscoll, and D. O. Scanlon, "Modulation of the Bi^{3+} $6s^2$ lone pair state in perovskites for high-mobility p-type oxide semiconductors," Adv. Sci. **9**(6), 2104141 (2022).
[59]Y. Yin, Y. Wu, G. Chen, and W.-J. Yin, "Double perovskite Ba_2BiTaO_6 as a promising p-type transparent conductive oxide: A first-principles defect study," J. Appl. Phys. **127**(17), 175703 (2020).
[60]A. Bhatia, G. Hautier, T. Nilgianskul, A. Miglio, J. Sun, H. J. Kim, K. H. Kim, S. Chen, G.-M. Rignanese, and X. Gonze, "High-mobility bismuth-based transparent p-type oxide from high-throughput material screening," Chem. Mater. **28**(1), 30–34 (2016).

[61]J. Willis and D. O. Scanlon, "Latest directions in p-type transparent conductor design," J. Mater. Chem. C **9**(36), 11995–12009 (2021).
[62]K. Yim, Y. Youn, M. Lee, D. Yoo, J. Lee, S. H. Cho, and S. Han, "Computational discovery of p-type transparent oxide semiconductors using hydrogen descriptor," npj Comput. Mater. **4**(1), 17 (2018).
[63]Y. Youn, M. Lee, D. Kim, J. K. Jeong, Y. Kang, and S. Han, "Large-scale computational identification of p-type oxide semiconductors by hierarchical screening," Chem. Mater. **31**(15), 5475–5483 (2019).
[64]J. C. Fan, K. Sreekanth, Z. Xie, S. Chang, and K. V. Rao, "p-type ZnO materials: Theory, growth, properties and devices," Prog. Mater Sci. **58**(6), 874–985 (2013).
[65]E.-C. Lee and K.-J. Chang, "Possible p-type doping with group-I elements in ZnO," Phys. Rev. B **70**(11), 115210 (2004).
[66]C. Park, S. Zhang, and S.-H. Wei, "Origin of p-type doping difficulty in ZnO: The impurity perspective," Phys. Rev. B **66**(7), 073202 (2002).
[67]Z. Ye, H. He, and L. Jiang, "Co-doping: An effective strategy for achieving stable p-type ZnO thin films," Nano Energy **52**, 527–540 (2018).